



Effects of indigo carmine concentration on the morphology and microwave absorbing behavior of PPy prepared by template synthesis

Shuchun Hu^{1,*}, Yu Zhou¹, Lingling Zhang¹, Sijin Liu², Kai Cui², Yaoyao Lu¹, Kainan Li¹, and Xiaodong Li¹

¹Key Laboratory of Advanced Technologies of Materials (Ministry of Education), School of Materials Science and Engineering, Southwest Jiaotong University, Chengdu 610031, China

²Key Laboratory of Transportation Tunnel Engineering (Ministry of Education), School of Civil Engineering, Southwest Jiaotong University, Chengdu 610031, China

Received: 24 May 2017

Accepted: 9 October 2017

Published online:

31 October 2017

© Springer Science+Business Media, LLC 2017

ABSTRACT

In the study, a series of polypyrrole (PPy) samples were prepared by a method of template synthesis at different indigo carmine (IC) concentrations while keeping the amount of pyrrole and FeCl₃ as well as the reaction conditions unchanged. Effects of IC concentration (M_{IC}) on the morphology, conductivity and microwave absorbing behavior of the obtained PPy products were investigated. The results showed that the morphology of PPy transformed from granular flocking to rods and then to spiral rods as M_{IC} increased from 0.05 to 7.50 mM, and the morphology transformation mechanism of PPy was attributed to the structural transformation of IC micelles caused by the change of M_{IC} . The conductivity of PPy was also found to be influenced by M_{IC} . Further investigation indicated that the spiral rod-shaped PPy (S-5) showed obviously superior microwave absorbing behavior compared with that of the granular flocking shaped PPy or that of the rod-shaped PPy, which was attributed to the benefits of its spiral structure and the comparably higher dielectric loss resulted from its lower conductivity.

Introduction

The past 20–30 years saw increasing concerns as well as significant achievements on the research of conducting polymers. Among diverse conducting polymers, polypyrrole (PPy), with high thermal and chemical stability, excellent conductivity and manageable synthesis, has been widely applied as a

functional material in electronic device manufacture. The application of PPy covers a wide range. For example, since it is reversible in doping, eco-friendly, high in specific capacitance and easy to form film, it has been used as an electrode material to produce supercapacitors [1–3] and rechargeable batteries [4, 5]. With electrical and gas sensitivity, PPy is also used to produce sensors [6, 7]. Some researchers have

Address correspondence to E-mail: schu@home.swjtu.edu.cn; shuchun_hu@sina.cn

tried to apply PPy to the chemical and electrochemical anticorrosion of metals by virtue of its functions of promoting the generation of passive oxide at the interfaces between metals and polymers, increasing the electrochemical corrosion potential of metals, transferring electrochemical corrosion interfaces and realizing controllable release of corrosion inhibitors [8–11]. There are also researchers who connected PPy with electromagnetic shielding [12–14] and microwave absorption [15, 16] in view of the dielectric loss mechanism and controllable electromagnetic parameters of PPy. However, a common problem faced by the above application fields is that the mentioned behaviors of PPy or its' composites are directly affected by its physical and chemical property parameters. Therefore, how to control these parameters of PPy has become a new research focus in recent years. Generally, the physical and chemical properties of PPy are adjusted by scholars from all over the world through adjusting the morphology and chemical structure of PPy [17–21], which is always based on the control over the synthesis method and reaction conditions. Among all the ways of PPy's synthesis, template synthesis is an effective way to regulate the morphology of PPy.

As far as hard templates are concerned, with using anodic aluminum oxide (AAO) membrane as the template, PPy nanotubule arrays were prepared by Liu et al. [22] through an electrochemical alternating current method, and the formation mechanism of PPy nanotubule arrays was mainly attributed to the limitation of AAO templates to the growth direction of PPy nanotubule after nuclei overlapping. With using Al_2O_3 nanoporous templates, doped and dedoped nanotubes and nanowires of polypyrrole, polyaniline and poly-(3,4-ethylenedioxythiophene) were synthesized by Kim et al. [23], and the possible applications of these nanotubes and nanowires in the construction of nanotip emitters in field emission displays and polymer-based transistors were presented. Fukami et al. [24] investigated electropolymerization of PPy into porous silicon template, and they obtained rod-shaped PPy arrays after removal of the templates. Moreover, they demonstrated that the size and the surface morphology of PPy rod were easily tuned using porous silicon.

Besides hard templates, more and more soft templates have been used in the template synthesis of PPy. With using methyl orange (MO) as the template and ammonium peroxy sulfate (APS) as the oxidant,

Dai et al. [25] prepared PPy microtubules at room temperature, and their researches demonstrated that the formation of PPy microtubules was a slow and self-assembled process. According to the report of Yang et al. [26], PPy nanotubes were synthesized by an in situ polymerization method with using a reactive self-degraded template (the fibrillary complex of FeCl_3 and MO), and the obtained PPy nanotubes were found to have high electric conductivity and azo function due to its hollow nanotubular structures. Lu et al. [27] synthesized fibrillar PPy on the cotton fabrics via a chemical polymerization process with micelles of cationic surfactant (cetyltrimethylammonium bromide, CTAB) as the soft templates. While FeCl_3 was used as the oxidant and Acid Red 1 was used as the dopant, aligned PPy micro/nanotubules were synthesized by Yan et al. [28], and the morphology of the obtained PPy could be manipulated by varying the synthetic conditions including polymerization time, monomer concentration, oxidant species and stirring. According to Ref. [28], the formation mechanism of rectangular-sectioned PPy micro/nanotubules was mainly attributed to AR1-Fe(II) complex (formed from the complexation of Acid Red 1 and Fe^{2+}), which might have functioned as 'template' during the polymerization of pyrrole monomers. Ralwal et al. [29] and Hazarika et al. [30] both reported the synthesis of PPy with using sodium dodecyl sulfate (SDS) as the template, and they all found that SDS concentration affected the morphologies of PPy. By changing SDS concentration in the range of 5–30 mM, Ralwal et al. [29] prepared elliptical and spherical PPy, respectively; Hazarika et al. [30] obtained spherical solid PPy nanoparticles (with SDS concentrations in the range of 0.01–0.2 M) and cylindrical PPy nanoparticles (at a SDS concentration of 0.5 M). As our early report [31], when indigo carmine (IC) and FeCl_3 were used as the dopant and oxidant, respectively, PPy in the morphology of spiral rods was synthesized via chemical oxidation method; Moreover, IC-Fe(II) chelate was proposed to be the synthesis template of PPy. In addition, as shown in Fig. 1, IC has short-chain planar molecular structure and both hydrophilic lipophilic groups [32]. Because of the well-known redox mechanism [33], the high extinction coefficient [34] and the dianionic character [32] of IC, it is beneficial to promote the electronic interaction with the π -system of PPy and finally promoting some photoelectrochemical properties of PPy. For example, with using IC as the

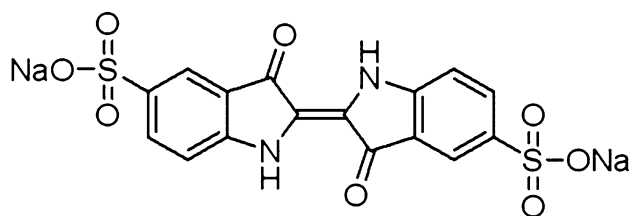


Figure 1 The molecular structure of IC [32].

dopant, Girotto et al. [35], Sultana et al. [32] and Loguercio et al. [36], respectively, reported their researches on PPy films (PPy-DS-IC film, PPy-IC film and PPy-IC-Au film, in order), which were all synthesized by electrochemical method, and the as-prepared PPy films showed relatively good electrochromic and photoelectrochemical properties [35], high discharge capacity [32] as well as enhanced electrochromic and optical properties [36].

According to the above literature survey and to our best knowledge, we are the main group focusing on spiral rod-shaped PPy prepared by chemical oxidation method as IC is used as the template. On the other hand, conductive polymers (including PPy) have been an important development direction of microwave absorbing materials, which is mainly ascribed to their outstanding lightweight characteristic. The density of PPy is about 1.2 g/cm^3 [37], less than one-sixth of that of steel, which makes PPy has the congenital technology advantage of lightweight compared with other microwave absorbers such as magnetic metal, ferrite and ceramic fibers. Certainly, it is also necessary to promote the microwave absorbing capability of PPy because microwave absorbers are always required to meet the overall performance requirements of lightweight, low thickness, strong absorption and wide absorption bandwidth. Much of the time, in order to enhance the absorption capability, PPy was compounded with magnetic materials [16, 38, 39] to prepare composited absorbers (including the core-shell-structured composites). Although the composite method is an effective way to promote the microwave absorbing property, the process will drastically increase the density of the absorbers. On the other side, spiral materials are good candidates for constructing efficient microwave absorbers with characteristics of lightweight, strong absorption and wide absorption bandwidth because of an additional more adjustable chiral parameter besides complex permittivity and permeability [40, 41].

Based on the above analysis and our previous work, still with IC as the synthesis template, PPy products with different morphologies (granular flocking, rods and spiral rods) were prepared in this paper through adjusting IC concentration in the reaction mixture. Based on the characterizations of PPy with different morphologies and the studies on the morphology transformation mechanism of the series of PPy products, the conductivity and microwave absorbing properties of PPy with different morphologies were emphatically investigated, which laid foundations for PPy's application in the area of lightweight microwave absorbing materials.

Experimental

Materials

Pyrrole ($\text{C}_4\text{H}_5\text{N}$, 98%) was purchased from Shanghai KF Chemical Reagent Co. Ltd (Shanghai, China). Indigo carmine ($\text{C}_{16}\text{H}_8\text{N}_2\text{Na}_2\text{O}_8\text{S}_2$, 95%), iron (III) chloride hexahydrate ($\text{FeCl}_3 \cdot 6\text{H}_2\text{O}$, 99%) and ethanol ($\text{C}_2\text{H}_6\text{O}$, 99.7%) were purchased from Chengdu Kelong Chemical Reagent Factory (Chengdu, China) and used as received. The water used in the experiments was distilled.

Synthesis of PPy at different IC concentrations

The process of PPy's synthesis is similar to that in our previous report [31], except for the use of different concentrations of IC. In general, while keeping the amount of pyrrole and FeCl_3 as well as the reaction conditions unchanged, six PPy samples were prepared at different IC concentrations (0.05, 0.10, 0.25, 0.75, 2.50 and 7.50 mM, in order) and marked as S-1, S-2, S-3, S-4, S-5 and S-6, in order. Taking S-1 as an example, it was prepared as follows: 0.0048 g IC was added to 180 ml distilled water and the obtained solution was hand stirred for 10 min to fully dissolve IC. Then, 1.38 ml pyrrole was added to the above solution, and the obtained miscible liquids (with an IC concentration of 0.05 mM) were transferred to an ice bath after hand stirring again to decrease its temperature to $5 \text{ }^\circ\text{C}$. Then, 20 ml of a previously confected FeCl_3 aqua (0.5 M) was dropwise added to the mixed liquids of pyrrole and IC in 20 min. The obtained mixture was still kept in the ice bath ($5 \text{ }^\circ\text{C}$)

condition to react for 9 h with slow magnetic stirring. Followed to the synthesis reaction, treatments such as decompression filtration, ethanol and distilled water washing and oven drying (45 °C, 12 h) were carried out and the final S-1 product in black powders was obtained.

Characterization of PPy synthesized at different IC concentrations

The morphologies of PPy samples were observed using a scanning electron microscopy (SEM, Inspect FEI, USA) at an accelerating voltage of 20.0 kV, and the powder was directly stuck on conductive tapes without dispersing before metal spraying and testing. With using a Fourier transform infrared spectrometer (FT-IR, Nicolet 6700, USA), the FT-IR spectra of IC and the as-prepared PPy products were recorded on a KBr pellet in a wavenumber range of 4000–400 cm^{-1} . The elementary composition of PPy products was qualitatively tested using an X-ray photoelectron spectroscopy (XPS, XSAM 800, Kratos). The conductivity of PPy was measured by a double electric four-probe multimeter (RTS-9, 4 Probes Tech, China). The electromagnetic parameters of PPy products were tested by a vector network analyzer (AV3672C, CETC, China) in the frequency range of 8–18 GHz.

Results and discussion

Morphological analysis of PPy synthesized at different IC concentrations

Figure 2 shows the SEM images of the PPy prepared at different IC concentrations.

As shown in Fig. 2a, when IC concentration (*abbr.* M_{IC}) was 0.05 mM, PPy in the morphology of granular flocking was obtained, and the average granule size of S-1 was 0.53 μm . When M_{IC} was doubled, the obtained S-2 still kept the morphology of granular flocking (as shown in Fig. 2b) and its average particle size decreased to 0.33 μm . As M_{IC} went up to 0.25 or 0.75 mM, rod-shaped PPy samples (S-3 and S-4) were prepared as shown in Fig. 2c, d. When M_{IC} stood at 2.50 or 7.50 mM, spiral rod-shaped PPy samples (S-5 and S-6) were obtained as shown in Fig. 2e, f. As far as the main morphology differentia between S-5 and S-6 was concerned, it could be observed that there

were obvious pitches between the spiral stripes of S-6, but the stripes of S-5 were close together.

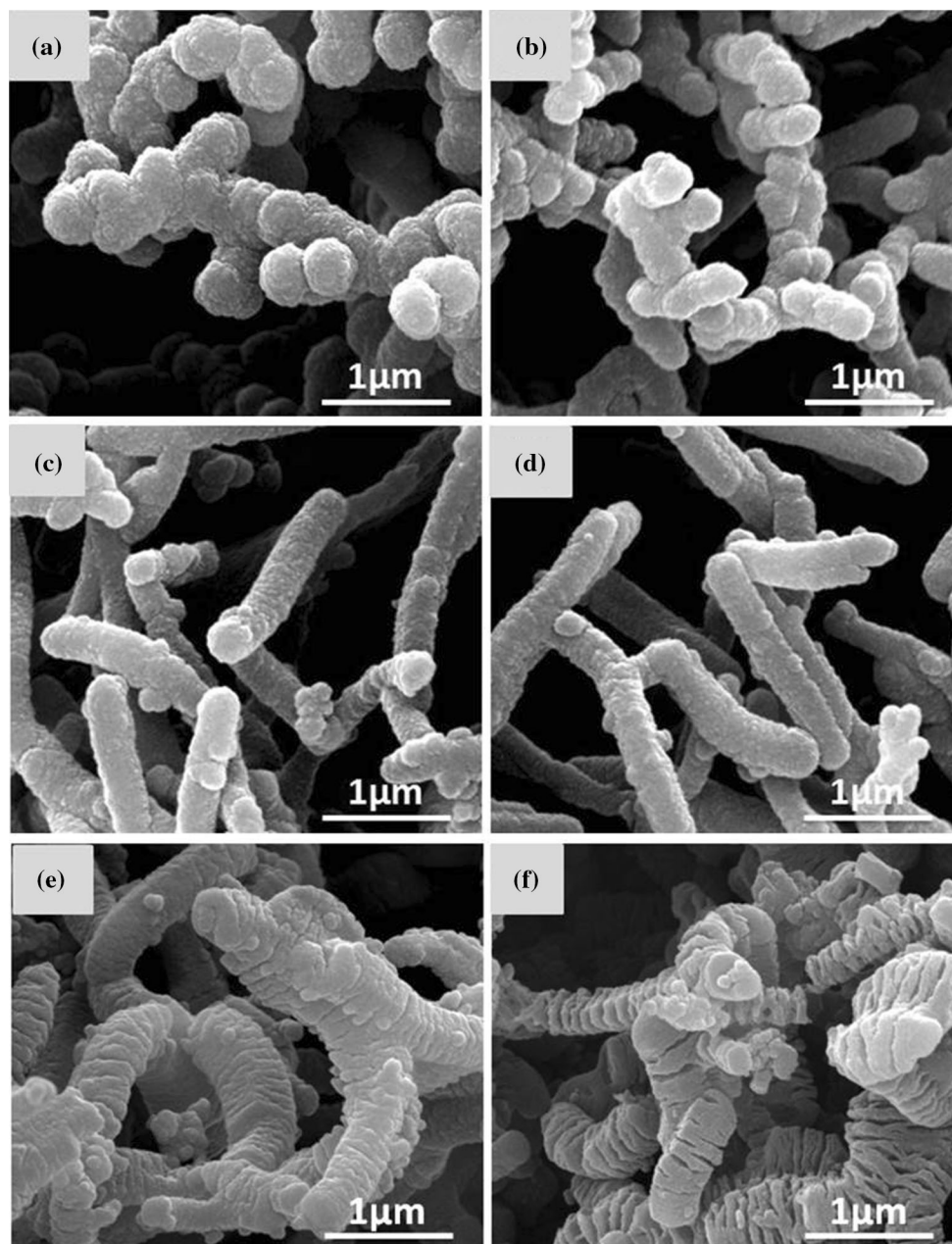
It can be thereby concluded that with the increase of M_{IC} , the morphology of PPy products turned from granular flocking to rods and then to spiral rods. These changes are related to the structural transformation of IC micelles (the synthesis templates of PPy) caused by the change of M_{IC} . The morphology transformation mechanism of PPy will be analyzed in detail hereinafter.

FT-IR and XPS analyses of PPy synthesized at different IC concentrations

Figure 3 shows the FT-IR spectra of pristine indigo carmine and PPy samples obtained at different M_{IC} . In the FT-IR spectrum of IC, the peak at 1700 cm^{-1} was assigned to the stretching vibration of C=O; the peaks at 1640 and 1611 cm^{-1} were related to the stretching vibration of C=C [42]; the peaks at 1471 and 1388 cm^{-1} were contributed to the stretching vibration of NH and C–C, respectively [43]; the peak at 1158 cm^{-1} was caused by C–H in plane bending vibration [42]; the peak at 1108 cm^{-1} was assigned to the stretching vibration of S=O [44]; the peak at 1037 cm^{-1} was contributed to the sulfonate anion vibration [36]; the peak at 824 cm^{-1} was caused by the C–H out-of-plane bending vibrations; the peaks at 731 and 678 cm^{-1} were related to C–N + S–O + C–C bending vibrations in plane; and C–N + S–O + C–C bending vibrations out of plane were at 588 cm^{-1} [42].

In the FT-IR spectra of PPy samples, the characteristic absorption peaks of PPy were observed at 1540, 1469, 1300, 1183, 964 and 778 cm^{-1} , respectively. Among these peaks, the peaks at 1540 and 1469 cm^{-1} were assigned to the C–C and C–N stretching vibration of pyrrole rings, and the peak at 1300 cm^{-1} was attributed to the C–H and C–N in-plane deformation [27]; the peak at 1183 cm^{-1} was caused by the C–N stretching vibration, and the peak at 964 cm^{-1} was related to the C–H out-of-plane vibration [37]; and the peak at 778 cm^{-1} was attributed to the C–H wagging vibration [45]. Therefore, it is suggested that the obtained products were PPy. In addition, the absorption peak of sulfonic acid group (1037 cm^{-1}) was also detected in the FT-IR spectra of S-1–S-6, which indicated that IC had been doped and grafted to the PPy chain [31, 46, 47]. This conclusion could be further proved by the supplementary proof

Figure 2 SEM images of PPy samples prepared at different M_{IC} . **a** S-1, $M_{IC} = 0.05$ mM; **b** S-2, $M_{IC} = 0.10$ mM; **c** S-3, $M_{IC} = 0.25$ mM; **d** S-4, $M_{IC} = 0.75$ mM; **e** S-5, $M_{IC} = 2.50$ mM; **f** S-6, $M_{IC} = 7.50$ mM.



of the XPS results (as shown in Fig. 4) because peaks of S and O elements were detected in the obtained XPS spectra of the representative PPy samples.

As shown in Fig. 3, the absorption peaks of the O–Fe–O (591 cm^{-1}) were detected in the FT-IR spectra of S-5 and S-6 which had the spiral rod-shaped morphology. As introduced in our previous report [31], the O–Fe–O formed as a result of the chelation of Fe^{2+} (reduced from Fe^{3+}) with the carbonyl oxygen of IC. Because of the chelation, cylindrical IC micelles transformed to spiral IC-Fe(II) chelate micelles, in which pyrrole was polymerized to PPy in the

morphology of spiral rods. This indicated that O–Fe–O contributed to the formation of spiral rod-shaped PPy.

The morphology transformation mechanism of PPy

As reported by us [31], since the PPy herein was prepared by taking IC micelles as synthesis templates, its morphology was mainly determined by the micelle structure. As is known to all, micelle is always in granular structure as the surfactant

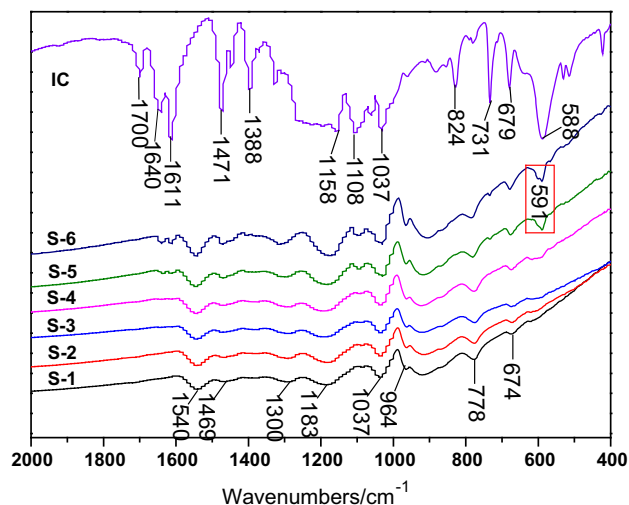


Figure 3 FT-IR spectra of IC and PPy samples prepared at different M_{IC} . S-1 M_{IC} = 0.05 mM; S-2, M_{IC} = 0.10 mM; S-3, M_{IC} = 0.25 mM; S-4, M_{IC} = 0.75 mM; S-5, M_{IC} = 2.50 mM; S-6, M_{IC} = 7.50 mM.

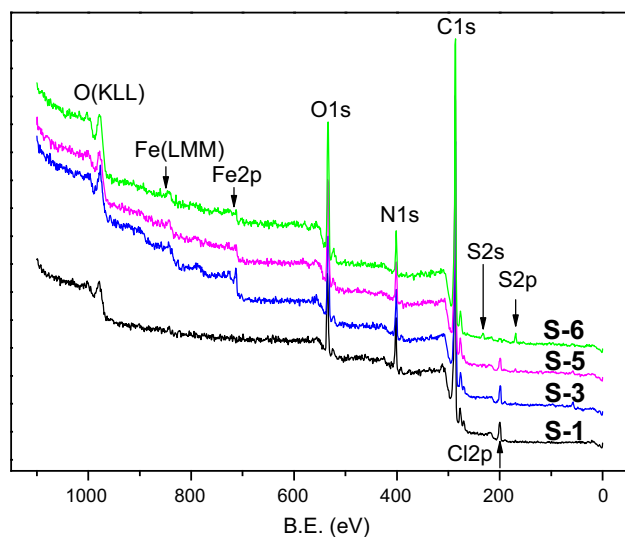


Figure 4 XPS spectra of the representative PPy samples. S-1, M_{IC} = 0.05 mM; S-3, M_{IC} = 0.25 mM; S-5, M_{IC} = 2.50 mM; S-6, M_{IC} = 7.50 mM.

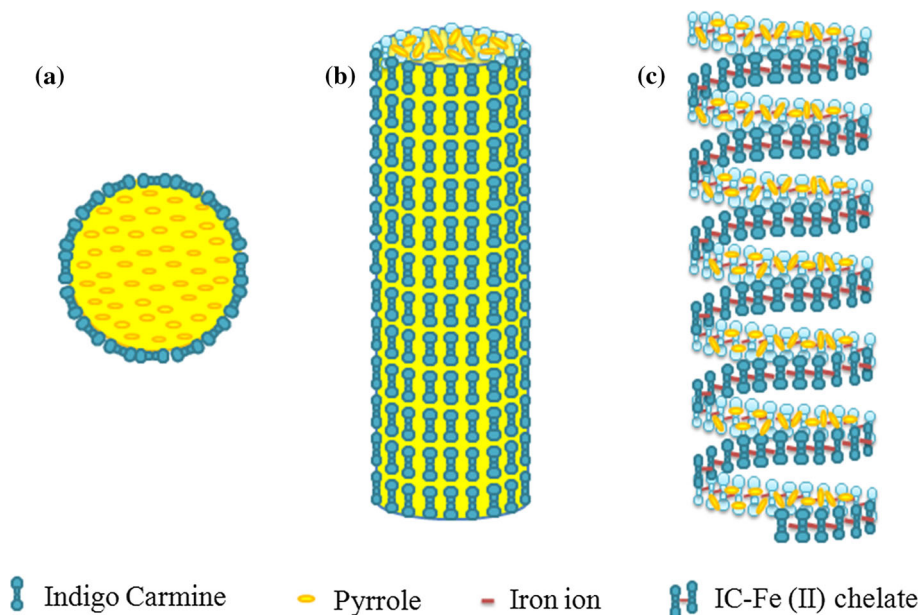
concentration is not too big [18, 48]. Therefore, when IC concentration was as low as 0.05 or 0.10 mM, granular IC micelles (Fig. 5a) formed with a big mole ratio of pyrrole to IC of 2000 or 1000. This meant that in the reaction system, a limited number of IC molecules surrounded a large amount of pyrrole monomers, forming granular micelles bonded by intermolecular forces. In these micelles, pyrrole was polymerized to granular flocking PPy as illustrated in Fig. 2a, b. As widely accepted, the structure of

surfactant micelle will gradually change from granular structure to rod-like or layered structure with the further increase in the surfactant concentration [18, 49]. So, it is possible that IC micelles transformed to be in rod structure (Fig. 5b) when IC concentration increased to 0.25 mM, which was corresponded to S-3 and five times as much as that of S-1. Thus, pyrrole was polymerized to rod-shaped PPy as shown in Fig. 2c. There are similar reports [50] on the relationship between surfactant concentration and micelle structure. When sodium dodecyl benzene-sulfonate (SDBS) is used as the surfactant, the micelle structure was changed from spherical to rod-like shape with the increase in SDBS concentration in the reaction system.

When IC concentration reached 2.50 mM, the morphology of micelles became spiral rod (Fig. 5c) and an obvious absorption peak of O–Fe–O (591 cm^{-1}) as a result of IC-Fe(II) chelation was observed in the FT-IR spectrum of S-5. According to our previous report [31], it is the chelation between the carbonyl oxygen of IC micelles and Fe^{2+} that contributes to the structure transformation of IC micelles from cylinder to spiral rod, in which pyrrole was polymerized to spiral rod-shaped PPy as shown in Fig. 2e. Similar analysis was also proposed by Kopecka et al. [51]. According to their report, methyl orange interacted with iron (III) salts to form the starting template of pyrrole's polymerization, and PPy nanotubes with circular or rectangular profiles were prepared.

It seemed that a faint absorption peak reflecting IC-Fe(II) chelation also appeared in the FT-IR spectrum of S-4; however, S-4 was not in the morphology of spiral rods, but rods (Fig. 2d) as S-3. It may be explained by the fact that the IC concentration (0.75 mM) for the formation of S-4 was much lower than that (2.50 mM) for the formation of S-5, and limited in number, IC molecules mainly participated in the formation of rod-shaped micelles instead of the chelation with Fe^{2+} which was the key point for the formation of spiral rod-shaped PPy. For the formation of S-5, it is greatly possible that the IC concentration was high enough to support the sufficient chelation of IC molecules with Fe^{2+} , so the structure of IC micelles changed from rods to spiral rods, and consequently, spiral rod-shaped PPy (Fig. 2e) was obtained. In addition, according to the XPS results, the S element composition (at%) of S-5 was 0.51%, which could be taken as a rough critical composition

Figure 5 Illustration of the structure transformation of micelles caused by the change of M_{IC} . **a** Granular micelle for S-1 and S-2 as M_{IC} was between 0.05 and 0.10 mM, **b** cylindrical micelle for S-3 and S-4 as M_{IC} was between 0.25 and 0.75 mM, **c** spiral rod micelle as M_{IC} was between 2.50 and 7.50 mM.



of S element for forming the spiral rod-shaped PPy. Moreover, compared with S-5, S-6 (as shown in Fig. 2f) is also in the morphology of spiral rods but with obvious stripe gaps. The reason is that increased IC concentration enhanced the chelation, which is possible to result in the pitch of spiral rod-like IC-Fe(II) chelate micelles and finally leads to the emerge of gaps between spiral stripes.

In conclusion, as the increase of M_{IC} , the structure of IC micelles transformed from granule to cylinder and then to spiral rod, and consequently, PPy products experienced the same transformation in morphology.

Effects of IC concentration to the conductivity of PPy

Figure 6 illustrates the curve of conductivity of PPy samples versus IC concentration. As shown in Fig. 6, it could be found that the conductivity of PPy rapidly decreased with the increase of M_{IC} when the value of M_{IC} was lower than 2.50 mM. As M_{IC} increased from 0.05 to 2.50 mM (from S-1 to S-5), the conductivity of the PPy decreased from 13.69 to 1.35 S/cm gradually. When M_{IC} further increased to 7.50 mM (S-6), the conductivity of S-6 rebounded to 5.36 S/cm.

According to the above data, it is suggested that M_{IC} is the main influencing factor on the conductivity of PPy. At a comparably lower M_{IC} condition, the doping level of chloridion was comparably higher because of the competition of chloridion and sulfonic

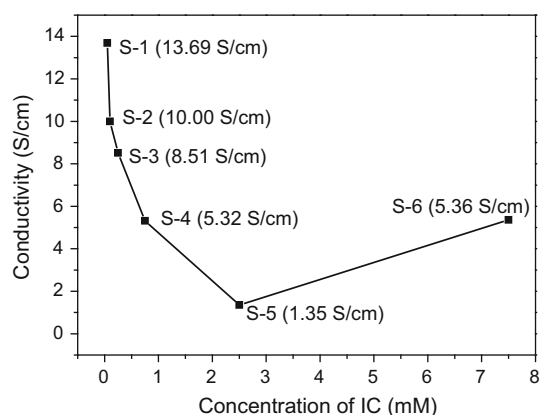


Figure 6 The curve of the conductivity of PPy (S-1 to S-6) versus IC concentration: S-1, $M_{IC} = 0.05$ mM; S-2, $M_{IC} = 0.10$ mM; S-3, $M_{IC} = 0.25$ mM; S-4, $M_{IC} = 0.75$ mM; S-5, $M_{IC} = 2.50$ mM; S-6, $M_{IC} = 7.50$ mM.

acid ion on doping to PPy molecular chain, and less IC molecule would be included in the PPy product, which could be proved by the at% of Cl and S elements (as shown in Table 1) of the representative PPy

Table 1 The at% of Cl and S elements of PPy samples

Sample	at% of Cl (%)	at% of S (%)
S-1	2.83	0.08
S-3	2.50	0.20
S-5	1.51	0.51
S-6	0.09	1.51

samples. The above two factors are both beneficial for promoting the conductivity of the product; therefore, it is reasonable that the conductivity of PPy rapidly decreases with the increase of M_{IC} in the range of 0.05–2.50 mM.

However, it is interesting and should be mentioned that the conductivity of PPy rose from 1.35 to 5.36 S/cm when M_{IC} was further increased from 2.50 to 7.50 mM (from S-5 to S-6). In consideration of the comparably higher content of IC of S-6 (the S elements contents of S-6 and S-5 were 1.51 and 0.51 at%, respectively) as well as the main morphology differentia between S-5 and S-6 (S-6 had obvious pitches between the spiral stripes, but the stripes of S-5 were close together), the main reason for S-6 showed a higher conductivity than that of S-5 was ascribed to pitches of spiral stripes in S-6. Because stripe pitches were beneficial for increasing the chance of PPy to expose from the outer layer of IC and providing PPy molecules more opportunities of direct contact, which contributed to transfer carrier between PPy rods as well as to increase the contact area of PPy molecules and reduce the contact resistance, thus finally resulted in the obvious increase in the conductivity of S-6. In addition, Genetti et al. [52] also reported a method to decrease the contact resistance which is increasing the contact area of PPy-coated nickel particles. This suggested that our conclusion is in accordance with Ref. [52].

Microwave absorbing behaviors of PPy products with different morphologies

In this paper, the permittivity and permeability of PPy products (S-1, S-3, S-5 and S-6) with different morphologies were tested by a vector network analyzer. Based on that, the reflection loss (RL) of different PPy products with a common defined specimen thickness of 1 mm are calculated according to Eqs. (1) and (2), and the calculated results are shown in Fig. 7.

$$Z = \sqrt{\frac{\mu}{\varepsilon}} \tanh \left[j \frac{2\pi}{\lambda} t \sqrt{\mu\varepsilon} \right] \tag{1}$$

$$RL = 20 \log \left| \frac{Z - 1}{Z + 1} \right| \tag{2}$$

Where Z is a complex number, ε and μ are the complex permittivity and permeability, respectively;

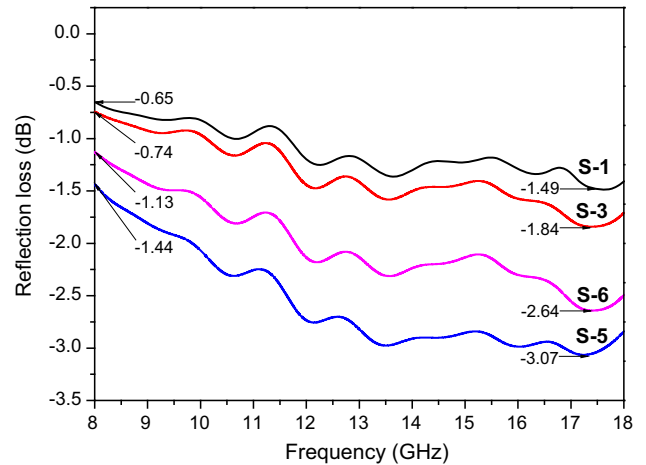


Figure 7 RL- f curves of PPy products (S-1, S-3, S-5 and S-6).

λ is the wavelength, t is the thickness of the specimen and $j = \sqrt{-1}$ [15, 53, 54].

It can be seen from Fig. 7 that among the three kinds of PPy products, those in the morphology of spiral rods (S-5 and S-6) appear obviously lower reflection loss (S-5: $-1.44 \sim -3.07$ dB; S-6: $-1.13 \sim -2.64$ dB) than that of the rod-shaped S-3 ($-0.74 \sim -1.84$ dB) and that of the granular flocking shaped S-1 ($-0.65 \sim -1.49$ dB), which suggests that the spiral structure of S-5 and S-6 is beneficial for promoting the microwave absorbing capability. According to the reports [55, 56] focusing on other spiral materials, spiral materials always have a certain extent of chiral characteristic, which can contribute to microwave absorption since it brings spiral materials an additional more adjustable chiral parameter besides complex permittivity and permeability [40, 41]. On the other hand, also because of the spiral structure, the polarization characteristic of the incident microwave will be significantly affected. Both self-polarization and cross-polarization will be resulted in, which is suggested to be another important reason for the increase in the microwave absorbing capability of spiral materials [56]. In addition, the obviously superior microwave absorbing behavior of spiral rod-shaped PPy is also related to their comparably lower conductivities to a certain extent, because a low conductivity is more beneficial for the formation of dipole and dielectric loss [47]. As far as the microwave absorbing comparison of S-5 and S-6 is concerned, the results (as shown in Fig. 7) clearly indicate that S-5 shows superior absorbing behavior than S-6 although they are both in spiral

rod-shaped morphology. According to the above analysis, the main reasons are suggested to be ascribed to the obviously lower conductivity of S-5 (1.35 S/cm) as compared with that of S-6 (5.36 S/cm), which increases dielectric loss to the incident microwave.

Conclusions

Six PPy samples were prepared at different M_{IC} while keeping the amount of pyrrole and $FeCl_3$ as well as the reaction conditions unchanged. As M_{IC} increased from 0.05 to 7.5 mM, the morphology of PPy transformed from granular flocking to rods and then to spiral rods. The morphology transformation mechanism of PPy was attributed to the structural transformation of IC micelles caused by the change of M_{IC} . The conductivity of PPy rapidly decreased with the increase of M_{IC} in the range of 0.05–2.50 mM; when M_{IC} further increased to 7.50 mM, the conductivity rebounded to 5.36 S/cm. The spiral rod-shaped PPy showed superior microwave absorbing behavior compared with that of the granular flocking shaped PPy or that of the rod-shaped PPy.

Acknowledgements

We would like to express our great thanks to the financial support from the following foundations: Opening Fund of High Technology Organic Fiber Key Laboratory of Sichuan Province (PLN 2016-09, PLN 2015-01).

Compliance with ethical standards

Conflict of interest The authors declare that they have no conflict of interest.

References

- Li S, Zhao C, Shu KW et al (2014) Mechanically strong high performance layered polypyrrole nano fibre/graphene film for flexible solid state supercapacitor. *Carbon* 79:554–562
- Xu JJ, Xiao T, Tan XY et al (2017) A new asymmetric aqueous supercapacitor: $Co_3O_4/Co_3O_4@polypyrrole$. *J Alloys Compd* 706:351–357
- Jian X, Li JG, Yang HM, Gao LL, Zhang EH, Liang ZH (2017) Carbon quantum dots reinforced polypyrrole nanowire via electrostatic self-assembly strategy for high-performance supercapacitors. *Carbon* 114:533–543
- Zhao Y, Zhu W, Chen GZ, Cairns EJ (2016) Polypyrrole/ TiO_2 nanotube arrays with coaxial heterogeneous structure as sulfur hosts for lithium sulfur batteries. *J Power Sources* 327:447–456
- Wu YW, Yokoshima T, Nara H, Momma T, Osaka T (2017) A pre-lithiation method for sulfur cathode used for future lithium metal free full battery. *J Power Sources* 342:537–545
- Shi WT, Liu CX, Song YL, Lin NS, Zhou S, Cai XX (2012) An ascorbic acid amperometric sensor using over oxidized polypyrrole and palladium nanoparticles composites. *Biosens Bioelectron* 38:100–106
- Joulazadeh M, Navarchian AH (2015) Ammonia detection of one-dimensional nano-structured polypyrrole/metal oxide nanocomposites sensors. *Synth Met* 210:404–411
- Martins JI, Reis TC, Bazzaoui M, Bazzaoui EA, Martins L (2004) Polypyrrole coatings as a treatment for zinc-coated steel surfaces against corrosion. *Corros Sci* 46:2361–2381
- González MB, Saidman SB (2011) Electrodeposition of polypyrrole on 316L stainless steel for corrosion prevention. *Corros Sci* 53:276–282
- Rahman SU (2011) Corrosion protection of steel by catalyzed polypyrrole films. *Surf Coat Technol* 205:3035–3042
- Grubač Z, Rončević IŠ, Metikoš-Huković M (2016) Corrosion properties of the Mg alloy coated with polypyrrole films. *Corros Sci* 102:310–316
- Gahlout P, Choudhary V (2016) Tailoring of polypyrrole backbone by optimizing synthesis parameters for efficient EMI shielding properties in X-band (8.2–12.4 GHz). *Synth Met* 222:170–179
- Ebrahimi I, Gashti MP (2016) Chemically reduced versus photo-reduced clay-Ag-polypyrrole ternary nanocomposites: comparing thermal, optical, electrical and electromagnetic shielding properties. *Mater Res Bull* 83:96–107
- Zhao H, Hou L, Lu YX (2016) Electromagnetic interference shielding of layered linen fabric/polypyrrole/nickel (LF/PPy/Ni) composites. *Mater Des* 95:97–106
- Xiao HM, Zhang WD, Fu SY (2010) One-step synthesis, electromagnetic and microwave absorbing properties of α - $FeOOH/polypyrrole$ nanocomposites. *Compos Sci Technol* 70:909–915
- Wang Y, Zhang WZ, Luo CY, Wu XM, Yan G, Chen WX (2016) Fabrication and high-performance microwave absorption of $Ni@SnO_2@PPy$ Core-Shell composite. *Synth Met* 220:347–355
- Wang YJ, Yang C, Liu P (2011) Acid blue AS doped polypyrrole (PPy/AS) nanomaterials with different morphologies as electrode materials for supercapacitors. *Chem Eng J* 172:1137–1144

- [18] Huang ZH, Hu SC, Zhang N, Chen XL, Chen D, Jin Q, Jian X (2012) Effect of volume ratio of acetonitrile to water on the morphology and property of polypyrrole prepared by chemical oxidation method. *Polym Eng Sci* 52:1601–1605
- [19] Wang JP, Tao XM, Li L (2014) Study on horn-shaped polypyrrole prepared by pulse potential. *Synth Met* 194:176–181
- [20] Zhai J, Li Y, Hu S, Xiao D, Han H, Jiang Y, Qu Y (2015) Effect of oxidant dosage and solvent ratio on electric properties of polypyrrole. *Mater Technol Adv Perf Mater* 3:90–95
- [21] Hazarika J, Kumar A (2016) Studies of structural, optical, dielectric relaxation and ac conductivity of different alkyl-benzenesulfonic acids doped polypyrrole nanofibers. *Phys B* 481:268–279
- [22] Liu L, Zhao C, Zhao Y et al (2005) Characteristics of polypyrrole (PPy) nano-tubules made by templated ac electropolymerization. *Eur Polym J* 41:2117–2121
- [23] Kim BH, Park DH, Joo J, Yu SG, Lee SH (2005) Synthesis, characteristics, and field emission of doped and de-doped polypyrrole, polyaniline, poly (3, 4-ethylenedioxythiophene) nanotubes and nanowires. *Synth Met* 150:279–284
- [24] Fukami K, Harraz FA, Yamauchi T, Sakka T, Ogata YH (2008) Fine-tuning in size and surface morphology of rod-shaped polypyrrole using porous silicon as template. *Electrochem Commun* 10:56–60
- [25] Dai T, Lu Y (2007) Water-soluble methyl orange fibrils as versatile templates for the fabrication of conducting polymer microtubules. *Macromol Rapid Commun* 28:629–633
- [26] Yang X, Zhu Z, Dai T, Lu Y (2005) Facile fabrication of functional polypyrrole nanotubes via a reactive self-degraded template. *Macromol Rapid Commun* 26:1736–1740
- [27] Lu M, Xie RY, Liu ZL, Zhao ZY, Xu H, Mao ZP (2016) Enhancement in electrical conductive property of polypyrrole-coated cotton fabrics using cationic surfactant. *J Appl Polym* 133:43601
- [28] Yan W, Han J (2007) Synthesis and formation mechanism study of rectangular-sectioned polypyrrole micro/nanotubules. *Polymer* 48:6782–6790
- [29] Rawal I, Kaur A (2014) Effect of anionic surfactant concentration on the variable range hopping conduction in polypyrrole nanoparticles. *J Appl Phys* 115:043717
- [30] Hazarika J, Kumar A (2013) Controllable synthesis and characterization of polypyrrole nanoparticles in sodium dodecylsulphate (SDS) micellar solutions. *Synth Met* 175:155–162
- [31] Li YB, Zhai J, Hu SC, Zhang CL, Cui J, Zheng MQ, Yuan YP (2015) Hexagonal spiral prismatic polypyrrole nanorods prepared by chemical oxidation. *Colloid Polym Sci* 293:329–332
- [32] Sultana I, Rahman MM, Wang JZ, Wang CY, Wallace GG, Liu HK (2012) Indigo carmine (IC) doped polypyrrole (PPy) as a free-standing polymer electrode for lithium secondary battery application. *Solid State Ion* 215:29–35
- [33] Fabian J, Hartman H (1980) *Indigoid Dyes. Light absorption of organic colorants*. Springer, Berlin, pp 115–136
- [34] Shen B, Olbrich-Stock M, Posdorfer J, Schindler RN (1991) An optical and spectroelectrochemical investigation of indigo carmine. *Z Phys Chem Short Commun* 173:251–255
- [35] Giroto EM, Gazotti WA, Tormena CF, Paoli MAD (2002) Photoelectronic and transport properties of polypyrrole doped with a dianionic dye. *Electrochem Acta* 47:1351–1357
- [36] Loguercio LF, Alves CC, Thesing A, Ferreira J (2014) Enhanced electrochromic properties of polypyrrole/indigo carmine/gold nanoparticles nanocomposite. *Phys Chem Chem Phys* 17:1234–1240
- [37] Khani O, Nemati F, Farrokhi H, Jazirehpour M (2016) Synthesis and characterization of electromagnetic properties of polypyrrole nanorods prepared via self-reactive MnO₂ template. *Synth Met* 220:567–572
- [38] Li YB, Chen G, Li QH, Qiu G, Liu X (2011) Facile synthesis, magnetic and microwave absorption properties of Fe₃O₄/polypyrrole core/shell nanocomposite. *J Alloys Compd* 09:4104–4107
- [39] Xu P, Han XJ, Wang C et al (2008) Synthesis of electromagnetic functionalized barium ferrite nanoparticles embedded in polypyrrol. *Phys Chem B* 112:2775–2781
- [40] Wang GZ, Gao Z, Tang SW et al (2012) Microwave absorption properties of carbon nanocoils coated with highly controlled magnetic materials by atomic layer deposition. *ACS Nano* 6:11009–11017
- [41] Zhao DL, Shen ZM (2008) Preparation and microwave absorption properties of carbon nanocoils. *Mater Lett* 62:3704–3706
- [42] El-Mansy MAM (2017) Quantum chemical studies on structural, vibrational, nonlinear optical properties and chemical reactivity of indigo carmine dye. *Spectrochim Acta Part A* 183:284–290
- [43] Han YQ, Shen MX, Zhu JJ, Wu Y, Zhang XG (2013) Preparation and capacitive performances of PEDOT/indigo carmine composite hydrogel. *Polym Compos* 34:989–996
- [44] Gaini LE, Lakraimi M, Sebbar E, Meghea A, Bakasse M (2008) Adsorption of indigo carmine dye by Mg–Al–CO₃ calcined layered double hydroxides. In: *Icton-Mw. IEEE*, pp 1–5
- [45] Shi W, Liang PF, Ge DT, Wang JX, Zhang QQ (2007) Starch-assisted synthesis of polypyrrole nanowires by a simple electrochemical approach. *Chem Commun* 23:2414–2416

- [46] Håkansson E, Lin T, Wang H, Kaynak A (2006) The effects of dye dopants on the conductivity and optical absorption properties of polypyrrole. *Synth Met* 156:1194–1202
- [47] Li YB, Jiang YM, Hu SC et al (2016) Control of morphology and electromagnetic properties of polypyrrole synthesized by the template method. *High Perf Polym* 28:225–230
- [48] Aloï A, Guibert C, Olijve LLC, Voets IK (2016) Morphological evolution of complex coacervate core micelles revealed by iPAINT microscopy. *Polymer* 107:450–455
- [49] Kumar S, Sharma D, Ghosh G, Kabir-ud-Din (2005) Structural modifications of aqueous ionic micelles in the presence of denaturants as studied by DLS and viscometry. *Langmuir* 21:9446–9450
- [50] González YI, Nakanishi H, Stjern Dahl M, Kaler EW (2005) Influence of pH on the micelle-to-vesicle transition in aqueous mixtures of sodium dodecyl benzenesulfonate with histidine. *J Phys Chem B* 109:11675–11682
- [51] Kopecká J, Kopecký D, Vršnáta M et al (2014) Polypyrrole nanotubes: mechanism of formation. *RSC Adv* 4:1551–1558
- [52] Genetti WB, Yuan WL, Grady BP, O'rear EA, Lai CL (1998) Polymer matrix composites: conductivity enhancement through polypyrrole coating of nickel flake. *J Mater Sci* 33:3085–3093. doi:[10.1023/A:1004387621165](https://doi.org/10.1023/A:1004387621165)
- [53] Truong VT, Riddell SZ, Muscat RF (1998) Polypyrrole based microwave absorbers. *Mater Sci* 33:4971–4976
- [54] Singh P, Babbar VK, Razdan A, Srivastava SL, Puri RK (2000) Complex permittivity, permeability, and X-band microwave absorption of CaCoTi ferrite composites. *J Appl Phys* 87:4362–4366
- [55] Liu L, He PG, Zhou KC, Chen TF (2013) Microwave absorption properties of helical carbon nanofibers-coated carbon fibers. *AIP Adv* 3:082112
- [56] Xu F, Ma L, Gan M et al (2014) Preparation and characterization of chiral polyaniline/barium hexaferrite composite with enhanced microwave absorbing properties. *J Alloys Compd* 593:24–29